IEEE Access
Multidisciplinary | Rapid Review | Open Access Journal

Received October 7, 2018, accepted October 28, 2018, date of publication October 31, 2018, date of current version November 30, 2018.

Digital Object Identifier 10.1109/ACCESS.2018.2878734

Wideband Polarization-Resolved Chaos With Time-Delay Signature Suppression in VCSELs Subject to Dual Chaotic Optical Injections

JIAN-JUN CHEN[1], YING-NI DUAN[1], LIN-FU LI[2], AND ZHU-QIANG ZHONG[3]

[1]School of Medical Engineering and Technology, Xinjiang Medical University, Ürümqi 830011, China
[2]School of Mechatronics Engineering, Guizhou Minzu University, Guiyang 550025, China
[3]School of Science, Chongqing University of Technology, Chongqing 400054, China

Corresponding author: Jian-Jun Chen (cjjliyan@163.com)

This work was supported by the National Natural Science Foundation of China under Grant 31760269, the Natural Science Foundation of Xinjiang Province of China under Grant 2018D01C162, and the Natural Science Foundation of Guizhou Province of China under Grant Qian Ke He Basic [2017]1082.

ABSTRACT Both the polarization-resolved chaotic bandwidth enhancement and time-delay signature suppression have been numerically investigated based on a slave vertical-cavity surface-emitting laser (S-VCSEL) driven by dual chaotic optical injections (DCOIs) from two master VCSELs (M-VCSELs) under optical feedbacks. The bandwidth and time-delay signature of polarization-resolved chaos generated in VCSELs are evaluated quantitatively via the effective bandwidth and autocorrelation function, respectively. The results show that, in contrast to the polarization-resolved chaos generated from S-VCSEL subject to single chaotic optical injection, for the equivalent injection conditions, the chaos generated by the DCOI configuration can simultaneously realize the bandwidth enhancement and time-delay signature suppression in the distinctly wider injection parameter spaces of injection strength and frequency detuning. By further exploring the influences of different injection parameters from two injection M-VCSELs on the bandwidth and time-delay signature of chaos, it is found that for the DCOI, the moderate injection strengths and relatively larger frequency detuning of two different injection paths are preferred to obtain the desired wideband polarization-resolved chaos with successful time-delay signature suppression.

INDEX TERMS Vertical cavity surface emitting lasers, dual chaotic optical injections, chaos, bandwidth, time-delay signature.

I. INTRODUCTION

As an inherent phenomenon in nature, chaos has been found in diverse fields of basic science such as mathematics, physical optics, chemistry, biology, neuron, and has gained much attention due to its application prospect [1]–[7]. Considerable efforts in recent years have been devoted to realize the control of chaos, especially the inhibition of harmful chaotic dynamics and the utilization of beneficial chaotic dynamics [8]. As one of the important branches of chaos, optical chaos based on semiconductor lasers (SLs) plays a significant role in high-speed secure communication, fast random number generation, chaotic lidar and radar, etc [9]–[17]. An external delayed optical feedback SL has been regarded as a main candidate for generating high dimensional complex chaos signals because of its feasible controllability and rich chaotic dynamics. Note that, in the previous reports, the bandwidth of optical chaos from the external delayed optical feedback SL was relatively low and typically possess several gigahertz (GHz) bandwidth, which may impose a negative effect on the performance of chaos-based applications [18], [19]. At the same time, chaotic signals from the delayed SL system are characterized intrinsically by the time-delay signature (TDS) which can be extracted from the intensity time series or phase time series of field. The retrospection of TDS will seriously intimidate the security of chaos-based secure communication [20], [21]. Moreover, the existence of TDS will also deteriorate the randomness of fast physical random bit sequences or restrict the resolution of chaotic lidar and radar [22], [23]. From the viewpoint of practical applications, high quality chaos is generally required to possess both the wide bandwidth and small TDS. As a result, how to widen the bandwidth and suppress the TDS of chaos in a delayed SL–based system has been a subject of considerable research effort.

In recent years, optimized feedback delayed SL systems, including the double optical feedbacks [24]–[26], polarized optical feedback [27], and grating feedback [28] have been utilized to obtain the high quality chaos. The related studies showed that the well-concealed TDS can be obtained through choosing the suitable feedback conditions. Because the external cavity disturbance process comes mainly from the feedback of the laser itself, these methods cannot remove the domination of relaxation oscillation frequency of SLs, and therefore the bandwidths of chaos from those systems remain relatively low. Since then, researchers have developed several strategies to solve the deficiency. For example, Wang et al. demonstrated that the broadband chaos can be achieved by injecting a continuous wave into a chaotic SL with the optical feedback [29]. Li *et al.* [30] reported the generation of wideband chaos with eliminated TDS by utilizing an optically injected master-slave system in which a slave SL is injected by a chaotic beam from a master SL subject to optical feedback. After that, by employing a cascade-coupled configuration involving three SLs (an external-cavity master SL, an intermediate SL, and a slave SL), they realized the simultaneous bandwidth enhancement and TDS suppression of chaos [31].

It is noteworthy that, related researchers have gradually shifted their focus on the case in which vertical-cavity surface-emitting lasers (VCSELs), a kind of very promising SL devices, are employed to be as an ideal light source, owing to their distinctive advantages such as low threshold current, circular beam profile, dynamical single-longitudinal mode operation, reduced manufacturing costs, easy fabrication in two-dimensional arrays [32], [33]. These particular properties of VCSELs motivate researchers to explore high quality chaos in VCSEL-based system. Recently, researchers experimentally and theoretically investigated the bandwidth enhancement of chaos in a chaotic slave VCSEL induced by the optical feedback and polarized optical injection from another master VCSEL [34]–[36]. Besides, some representative research has been focused and devoted on simultaneous bandwidth enhancement and TDS suppression of chaos in the VCSEL-based system [37], [38]. Hong *et al.* [37] experimentally reported that the enhanced bandwidth and suppressed TDS of chaos can be achieved simultaneously in two different VCSEL configurations–a mater-slave system associated with chaotic optical injection and a mutually coupled system involving a solitary VCSEL and an external-cavity chaotic VCSEL. Subsequently, through adopting three-cascaded VCSELs configuration, they experimentally demonstrated that the wideband chaos with totally suppressed TDS can be obtained from the third laser when the injection chaos from the middle VCSEL has an intermediate bandwidth and relatively low TDS [38]. The above results show that the chaotic optical injection is a feasible technical route to simultaneously promote the bandwidth and eliminate TDS of chaos in the delayed VCSEL system. Moreover, some studies have proven that dual chaotic optical injection (DCOI) can heighten the unpredictability degree of chaos in a delayed SL-based system [39]. Particularly, further bandwidth enhancement can be realized over a wider parameters regime compared with the case of single chaotic optical injection (SCOI) [40], [41]. However, we have noticed that, little work has been undertaken to simultaneously optimize the bandwidth and TDS of chaos in a delayed VCSEL-based system subject to DCOI. Different from conventional SLs mentioned above, VCSELs can output two linearly polarized lights along two orthogonal crystal axes owing to weak material and cavity anisotropies, which results in the generated chaotic signals with polarization reliance. Polarized chaotic lights with wide bandwidth and low TDS are preferred for some polarization-sensitive applications.

In this paper, a DCOI configuration is adopted for generating polarization-resolved wideband chaos with TDS suppression based on a slave VCSEL (S-VCSEL) driven by two injected chaos beams from two master VCSELs (M-VCSEL1 and M-VCSEL2) under respectively optical feedbacks. The effects of injection parameters on both the bandwidth and TDS of polarized chaos from this system are numerically investigated, and the appropriate parameter regions for simultaneously achieving the bandwidth enhancement and successful TDS concealment are identified.

II. SYSTEM MODEL AND THEORY

The schematic diagram of the proposed DCOI system configuration is shown in Fig. 1. Here, the two chaotic beams from the master VCSEL1 and VCSEL2 (M-VCSEL1 and M-VCSEL2) are respectively generated through external optical feedback from the mirror1 and mirror2 (M1 and M2), and then unidirectionally injected into the slave VCSEL (S-VCSEL) after passing through the beam splitters (BSs), neutral density filters (NDFs), and optical isolators (ISOs) of respective path. In this system, NDF1 and NDF2 are used to adjust the injection strength of two injection paths, respectively, and ISO1 and ISO2 of two paths are employed to guarantee light unidirectional injection. To clarify differences, the case for SCOI is also presented to compare with that of DCOI. For SCOI, the devices within the dashed lines should be removed.

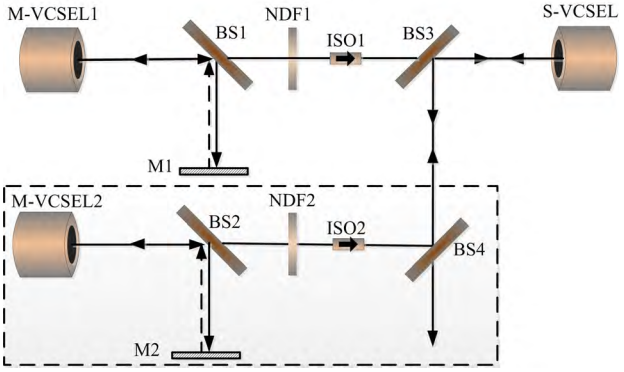

FIGURE 1. Schematic diagram of the VCSEL subject to DCOI. M-VCSEL1, 2: master VCSEL1, 2; S-VCSEL: slave VCSEL; M: mirror; NDF: neutral density filter; BS: beam splitter; ISO: optical isolator.

Based on the spin-flip model (SFM) [32], the rate equations for M-VCSEL1 and M-VCSEL2 under optical feedbacks and S-VCSEL under DCOI can be written as:

$$\begin{aligned}\frac{dE_{x,y}^{M1,M2}}{dt} &= k^{M1,M2}(1+i\alpha^{M1,M2})[(N^{M1,M2}\\ &-1)E_{x,y}^{M1,M2} \pm in^{M1,M2}E_{y,x}^{M1,M2}] \mp (\gamma_a^{M1,M2}\\ &-i\gamma_p^{M1,M2})E_{x,y}^{M1,M2} + \sqrt{\beta_{sp}}\xi_{x,y}^{M1,M2}\\ &+k_f E_{x,y}^{M1,M2}(t-\tau_f)e^{-i2\pi\nu^{M1,M2}\tau_f} \qquad (1)\end{aligned}$$

$$\begin{aligned}\frac{dE_{x,y}^{S}}{dt} &= k^{S}(1+i\alpha^{S})[(N^{S}-1)E_{x,y}^{S} \pm in^{S}E_{y,x}^{S}]\\ &\mp(\gamma_a^{S}+i\gamma_p^{S})E_{x,y}^{S} + \sqrt{\beta_{sp}}\xi_{x,y}^{S}\\ &+\eta_{SCOI}E_{x,y}^{M1}(t-\tau_\eta)e^{-i2\pi\nu^{M}\tau_\eta+i2\pi\Delta\nu t}\\ &+\eta_1 E_{x,y}^{M1}(t-\tau_{\eta1})e^{-i2\pi\nu^{M1}\tau_{\eta1}i2\pi\Delta\nu_1 t}\\ &+\eta_2 E_{x,y}^{M2}(t-\tau_{\eta2})e^{-i2\pi\nu^{M2}\tau_{\eta2}+i2\pi\Delta\nu_2 t} \qquad (2)\end{aligned}$$

$$\begin{aligned}\frac{dN^{M1,M2,S}}{dt} &= -\gamma_e^{M1,M2,S}[N^{M1,M2,S}(1+|E_x^{M1,M2,S}|^2\\ &+|E_y^{M1,M2,S}|^2) - u^{M1,M2,S}\\ &+in^{M1,M2,S}(E_y^{M1,M2,S}E_x^{M1,M2,S*}\\ &-E_x^{M1,M2,S}E_y^{M1,M2,S*})] \qquad (3)\end{aligned}$$

$$\begin{aligned}\frac{dn^{M1,M2,S}}{dt} &= -\gamma_s^{M1,M2,S}n^{M1,M2,S} - \gamma_e^{M1,M2,S}\\ &\times[n^{M1,M2,S}(|E_x^{M1,M2,S}|^2+|E_y^{M1,M2,S}|^2)\\ &+iN^{M1,M2,S}(E_y^{M1,M2,S}E_x^{M1,M2,S*}\\ &-E_x^{M1,M2,S}E_y^{M1,M2,S*})] \qquad (4)\end{aligned}$$

where the superscripts $M1$, $M2$ and S correspond to M-VCSEL1, M-VCSEL2 and S-VCSEL, respectively, and the subscripts x and y stand for X polarization component (X-PC) and Y polarization component (Y-PC), respectively. E is the slowly varied complex amplitude of the optical field, N is the total carrier inversions between the conduction and valence bands, n accounts for the difference between carrier channels, k is the field decay rate, α is the line-width enhancement factor, γ_e is the decay rate of N, γ_s is the spin-flip rate, and γ_a and γ_p are the linear dichroism and birefringence, respectively. k_f is the feedback strength, and τ_f is the corresponding feedback delay time. In equation (2), the fourth term corresponds to the case of SCOI which represents the injection only from M-VCSEL1 into S-VCSEL, where η_{SCOI} and τ_η are the injection strength and delay time, respectively, meanwhile $\Delta\nu$ is frequency detuning between M-VCSEL1 and S-VCSEL. The fifth and sixth terms correspond to the case of DCOI, where η_1 (η_2) characterizes the injection strength from M-VCSEL1 (M-VCSEL2) to S-VCSEL, $\tau_{\eta1}$ ($\tau_{\eta2}$) denotes the corresponding injection delay time, and $\Delta\nu_1 = \nu_1 - \nu_S$ ($\Delta\nu_2 = \nu_2 - \nu_S$) is the frequency detuning between M-VCSEL1 (M-VCSEL2) and S-VCSEL (ν_1, ν_2 and ν_S are the central frequency of M-VCSEL1, M-VCSEL2 and S-VCSEL, respectively). β_{sp} is the spontaneous emission factor, and ξ is the Gaussian white noise terms of zero mean value and unitary variance. u is the normalized bias current (u takes 1 at threshold).

In general, the bandwidth of chaotic signal is defined to be equal to the frequency at which 80% of the total power is contained within the power spectrum [42]. However, the amplitude of the low frequency region near DC in the power spectrum is usually smaller than that of the laser relaxation resonance peak. Hence the bandwidth based on the above definition is sometimes overestimated. Here, in order to ensure the effectiveness of the calculated chaotic signal bandwidth, the effective bandwidth (EBW) proposed by Lin *et al.* [43], which sums up only those discrete spectral segments of the chaotic power spectrum accounting for 80% of the total power, is adopted to realize the measurement of chaos bandwidth.

The autocorrelation function (ACF) is used to quantitatively evaluate the TDS in this paper and can be defined as [20]:

$$C(\Delta t) = \frac{\langle (I(t+\Delta t) - \langle I(t)\rangle)\,(I(t) - \langle I(t)\rangle)\rangle}{\sqrt{\left\langle (I(t+\Delta t) - \langle I(t+\Delta t)\rangle)^2\right\rangle \left\langle (I(t) - \langle I(t)\rangle)^2\right\rangle}} \qquad (5)$$

where $I(t)$ represents the output intensity of the VCSEL, $<\cdot>$ denotes time average, Δt is the time interval between two intensities. The TDS can be identified by evaluating the peak location and amplitude of the ACF curve.

III. RESULTS AND DISCUSSION

The equations (1)-(4) can be solved numerically with the fourth-order Runge-Kutta method. During the calculations, the intrinsic parameters of solitary M-VCSEL1, M-VCSEL2 and S-VCSEL are assumed to be identical and set as follows [44], [45]: $k = 300\ \text{ns}^{-1}$, $\alpha = 3$, $\gamma_e = 1\ \text{ns}^{-1}$, $\gamma_s = 50\ \text{ns}^{-1}$, $\gamma_a = 0.1\ \text{ns}^{-1}$, $\gamma_p = 10\ \text{ns}^{-1}$, $\beta_{sp} = 10^{-6}$, and the central frequency of the free-running VCSEL is 3.52941×10^{14} Hz (corresponding to 850 nm). Other parameters are: $k_f = 15\ \text{ns}^{-1}$, $\tau_f = 3$ ns, $\tau_{\eta1} = \tau_{\eta2} = 0$ ns. The normalized bias current u is chosen at 2.7 for that X-PC and Y-PC in the solitary VCSEL possess similar average intensity [45]. Under this circumstance, the relaxation oscillation frequency $f_{RO}(= \sqrt{2k\gamma_e(u-1)}/2\pi)$ of the solitary VCSEL is about 5.08 GHz.

For the purpose of comparison, we illustrate the time series, optical spectra, power spectra, and corresponding ACF curves of the X-PC and Y-PC outputs from M-VCSEL1 with optical feedback (a1-a8), S-VCSEL with SCOI (b1-b8) and S-VCSEL (c1-c8) with DCOI in Fig. 2. The first, second, third, and fourth rows are for the time series, optical spectra, power spectra, and ACF curves, respectively. Here, in order to ensure the comparability between SCOI and DCOI, the frequency detuning for SCOI and DCOI are all fixed at the same value of -20 GHz ($\Delta\nu = -20$ GHz, $\Delta\nu_1 = \Delta\nu_2 = -20$ GHz). The same treatment is also applied to injection strengths for SCOI and DCOI, where η_{SCOI} is equal to the effective total injection strength η_{DCOI} expressed as $\eta_{DCOI} = \eta_1 + \eta_2$ ($\eta_{SCOI} = 80\ \text{ns}^{-1}$, $\eta_{DCOI} = 80\ \text{ns}^{-1}$ with $\eta_1 = \eta_2$).

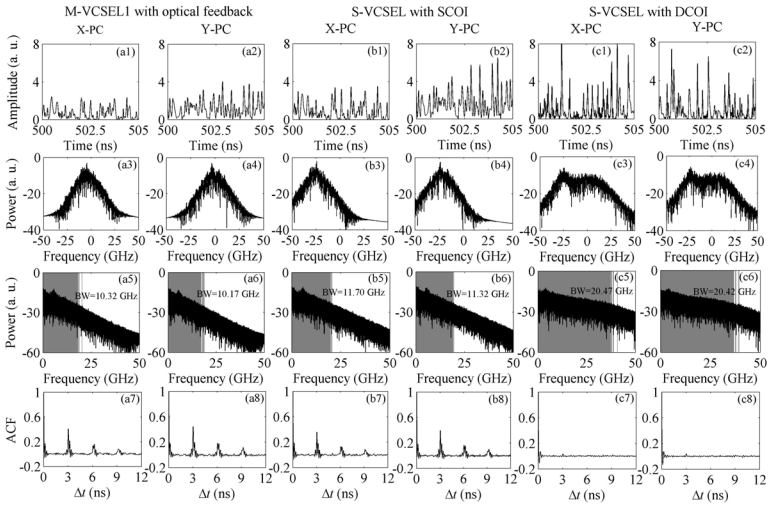

FIGURE 2. Time series (first row), optical spectra (second row), power spectra (third row), and corresponding ACF curves (fourth row) of polarization-resolved outputs. (a1-a8): M-VCSEL1 with optical feedback; (b1-b8): S-VCSEL with SCOI; and (c1-c8): S-VCSEL with DCOI. The corresponding parameters are $\Delta\nu = -20$ GHz, $\eta_{SCOI} = 80$ ns^{-1}, $\Delta\nu_1 = \Delta\nu_2 = -20$ GHz, and $\eta_{DCOI} = 80$ ns^{-1} with $\eta_1 = \eta_2 = 40$ ns^{-1}.

The shaded areas in the power spectra (third row) denote the spectral spans which sum up only those discrete spectral segments accounting for 80% of the total power. As shown in the first row of Fig. 2, the time series of X-PCs and Y-PCs in M-VCSEL1 with optical feedback, S-VCSEL with SCOI or DCOI show the random intensity pulsing, which indicates that the lasers operate in chaotic dynamics. For the case of M-VCSEL1 with optical feedback (Fig. 2(a1)-(a8)), the optical spectra of X-PC and Y-PC of M-VCSEL1 are typical chaos shapes with the broad peak, the power spectra have a peak centered around 5.08 GHz related with the relaxation oscillations and possess the EBWs of 10.32 GHz and 10.17 GHz for X-PC and Y-PC, respectively, and the corresponding ACF curves present the obvious TDS peaks at around τ_f, $2\tau_f$, and $3\tau_f$. For the case of S-VCSEL with SCOI (Fig. 2(b1)-(b8)), one can see that the intensity pulsing of the time series of X-PC and Y-PC of S-VCSEL are basically synchronized to those of M-VCSEL, which is originated from the injection locking mechanism. The optical spectra of X-PC and Y-PC of S-VCSEL display the similar peak structure with those of M-VCSEL, which is close to the emitting frequency of corresponding polarization components in the injecting M-VCSEL1. As a result, the EBWs of two polarization components from S-VCSEL are only slightly enhanced to 11.70 GHz and 11.32 GHz, respectively. Accordingly, the TDS associated with the ACF peak only attenuates moderately and can still be easily identified. Interestingly, for the case of S-VCSEL with DCOI (Fig. 2(c1)-(c8)), under the equivalent injection conditions, injection locking effect cannot be realized between M-VCSELs and S-VCSEL. The optical spectra of X-PC and Y-PC of S-VCSEL become much broad in the frequency range. The power spectra are flatter than the case for S-VCSEL with SCOI, and the corresponding EBWs of X-PC and Y-PC can be significantly increased to 20.47 GHz and 20.68 GHz, respectively. Meanwhile, the TDSs in the ACF curves for two orthogonal polarizations have almost been depressed into the background fluctuation. This shows that, under appropriate injection conditions, such a DCOI configuration can afford a possible way for simultaneously achieving the enhanced bandwidth and suppressed TDS of chaos.

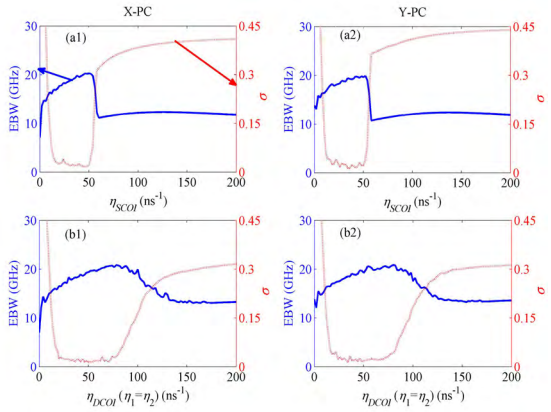

FIGURE 3. The EBW and σ of the polarization-resolved outputs as a function of η_{SCOI} for S-VCSEL with SCOI (a1, a2) and η_{DCOI} ($\eta_1 = \eta_2$) for S-VCSEL with DCOI (b1, b2), respectively. The corresponding parameters are $\Delta\nu = -20$ GHz and $\Delta\nu_1 = \Delta\nu_2 = -20$ GHz.

Figure 3 further presents the EBW and TDS of polarization-resolved chaotic outputs as a function of η_{SCOI} for S-VCSEL with SCOI (a1, a2) and η_{DCOI} ($\eta_1 = \eta_2$) for S-VCSEL with DCOI (b1, b2), respectively. $\Delta\nu$, $\Delta\nu_1$ and $\Delta\nu_2$ are all fixed at -20 GHz. Here, the peak value σ of the ACF curves within [3.5 ns, 4.5 ns] is used to evaluate the TDS. The blue and red lines represent the EBW and σ, respectively.

The larger σ is, the more obvious the TDS will be. For the case of S-VCSEL with SCOI (Fig. 3(a1)-(a2)), the chaotic injection from M-VCSEL1 firstly forces S-VCSEL into the chaotic dynamics, leading to the rapid increase of EBWs of the polarization-resolved outputs. As η_{SCOI} gradually increases, EBWs further increase, which can be attributed to enhanced relaxation oscillation frequency induced by optical injection. With further increase of η_{SCOI}, EBWs reach a maximal value and then quickly decrease until η_{SCOI} is beyond 55 ns^{-1}, indicating the injection locking effect at the relatively small injection strength. Correspondingly, within the EBW enhanced region, the low σ ($\sigma < 0.1$) is also found at the range of 10 ns^{-1} $< \eta_{SCOI} <$ 55 ns^{-1} where the TDS can be well suppressed. For the case of S-VCSEL with DCOI (Fig. 3(b1)-(b2), though the evolution trends of EBWs and TDSs for X-PC and Y-PC outputs are partly similar to the case for the SCOI, the wider region in the η_{DCOI} range can be obtained for achieving both the enhancement of EBW and concealment of TDS of chaotic signal. The injection locking between M-VCSELs and S-VCSEL cannot be realized under the relatively low η_{SCOI} conditions. The reason is that the DCOI configuration complexes the freedom degree of the system which contributes to more red-shift of cavity resonance and meanwhile weakens the periodical TDS of chaotic signals caused by the external optical feedback.

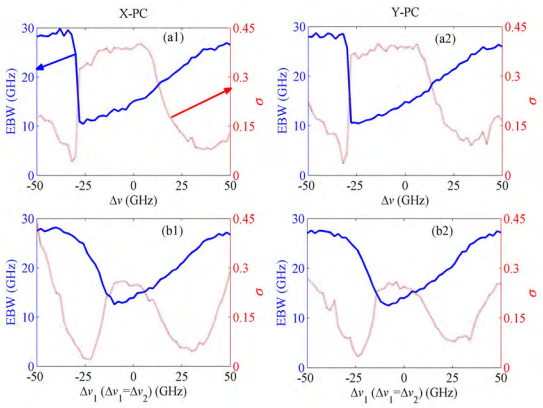

FIGURE 4. The EBW and σ of the polarization-resolved outputs as a function of $\Delta\nu$ for S-VCSEL with SCOI (a1, a2) and $\Delta\nu_1$ ($\Delta\nu_1 = \Delta\nu_2$) for S-VCSEL with DCOI (b1, b2), respectively. The corresponding parameters are $\eta_{SCOI} = 80$ ns^{-1} and $\eta_{DCOI} = 80$ ns^{-1} with $\eta_1 = \eta_2$.

Next, the influences of frequency detuning on the EBW and σ are also taken into consideration. Figure 4 shows the dependence of EBW and σ of the polarization-resolved outputs as a function of $\Delta\nu$ for S-VCSEL with SCOI (a1, a2) and $\Delta\nu_1$ ($\Delta\nu_1 = \Delta\nu_2$) for S-VCSEL with DCOI (b1, b2), respectively. The injection strength η_{SCOI} for SCOI and η_{DCOI} for DCOI are both fixed at 80 ns^{-1}. In Fig. 4(a1)-(a2), when the SCOI is adopted, the regions with relatively high EBW for X-PC and Y-PC mainly exist in the range of $|\Delta\nu| >$ 25 GHz. Once $\Delta\nu$ is close to 25 GHz or set to small values, the injection locking effect results in a rapid reduction of EBW. Note that, only two very small regions with low σ($\sigma < 0.1$) are identified around -32 GHz and 37GHz, respectively. As a result, the overlapped regions for both the bandwidth enhancement and TDS suppression must satisfy the strict parameter condition. However, from Fig. 4(b1)-(b2), one can see that, DCOI with equivalent injection strength exert a different effect on the EBW and TDS of polarization-resolved chaos. $\Delta\nu_1$ ($\Delta\nu_2$) corresponding to the injection locking shifts to the smaller value than the case of SCOI, which are benefit from the weakened injection locking effect originated from DCOI. The low σ($\sigma < 0.1$) can be obtained at two valleys in the negative and positive frequency detuning range, respectively. The optimized overlapped range can cover wider detuning regions compared with that for the SCOI case.

To comprehensively reveal the influence of both injection strength and the frequency detuning on the bandwidth as well as TDS, two dimensional maps of EBW (a1-a4) and σ (b1-b4) for S-VCSEL with SCOI (first row) and with DCOI (second row) in the parameter space of injection strength and frequency detuning are respectively presented in Fig. 5, to identify the optimal operating parameter regions for successful bandwidth enhancement and TDS suppression. In the EBW (σ) maps, different colors correspond to different chaotic bandwidths (different TDS level), and the black (white) dashed lines represent the parameter location of EBW (σ) with 20 GHz (0.1). These dashed lines divide the EBW (σ) into different regions. For the case of S-VCSEL with SCOI (Fig. 5(a1)-(a2)), the marked regions with the deep blue color correspond to the small EBWs less than 15 GHz, where S-VCSEL with SCOI operates at the injection locking state mainly located in the negative detuning position. The higher EBWs more than 20 GHz concentrate at the specific regions of parameter space characterized by the yellow and red colors. Combining with the σ maps presented in Fig. 5(b1)-(b2), one can observe that, the low σ ($\sigma < 0.1$) for X-PC and Y-PC covers a narrow shape as the letter 'V' which partially coincides with the parameter regions with the wide EBWs shown in Fig. 5(a1)-(a2). The above results are similar to those obtained in [37]. Nevertheless, optimized overlapped regions in the parameter space are relatively small and the parameters must be carefully chosen to meet the requirement of both the wide bandwidth and low TDS. For the case of S-VCSEL with DCOI (Fig. 5(a3)-(a4)), $\Delta\nu_1$ and $\Delta\nu_2$ are the same value, and η_{DCOI} is set to be equal to η_{SCOI}. As shown in the diagrams, the distribution of EBW of the polarization-resolved outputs from the S-VCSEL with DCOI are different from the case of SCOI, and the parameter regions corresponding to enhanced EBW becomes much wider. Apparently, the injection locking region is significantly reduced, especially in the range of negative detuning. This can be explained that, though the parameters of M-VCSEL1 and M-VCSEL2 have the same values, different initial conditions for the two lasers still can lead to generation of different chaotic dynamics and more frequency components due to frequency beating between the two injected optical field and the S-VCSEL field,

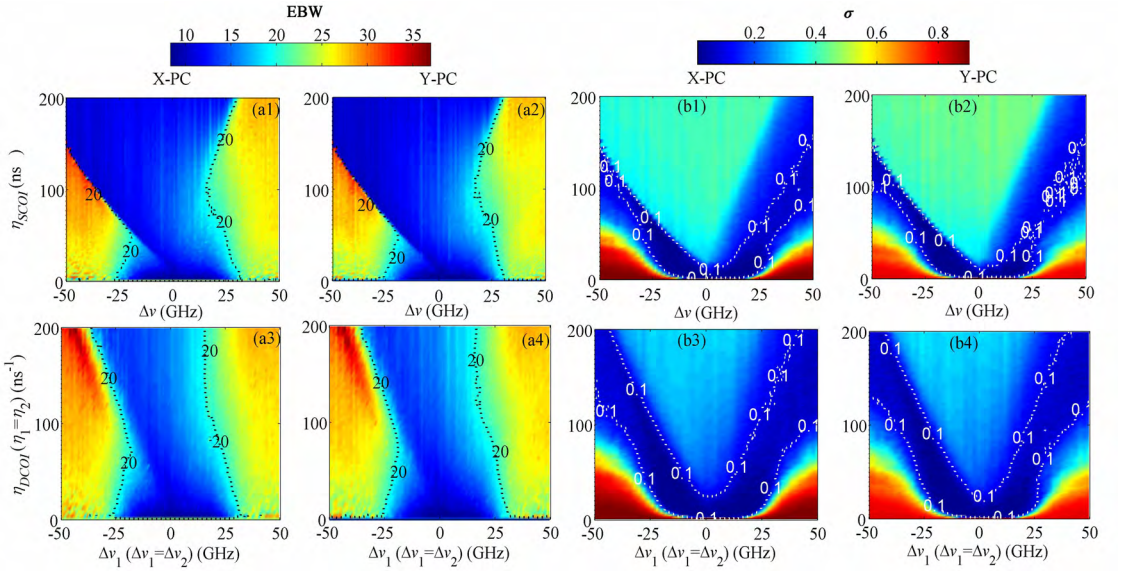

FIGURE 5. Evolution maps of EBW (a1-a4) and σ (b1-b4) of the polarization-resolved outputs of S-VCSEL. (first row): S-VCSEL with SCOI in the parameter space of η_{SCOI} and $\Delta\nu$; and (second row): S-VCSEL with DCOI in the parameter space of η_{DCOI} and $\Delta\nu_1$ ($\Delta\nu_1 = \Delta\nu_2$). The corresponding parameters are set as $\Delta\nu_1 = \Delta\nu_2$ and $\eta_1 = \eta_2$.

which weakens the injection locking effect. At the same time, it can be seen from Fig. 5(b3)-(b4), the 'V' areas with low σ ($\sigma < 0.1$) are expanded significantly for X-PC and Y-PC. In this case, the bandwidth enhancement and TDS suppression of polarization-resolved chaos can be simultaneously achieved in the wider parameter regions compared to the case of SCOI. It further indicates that, for suitable system parameters, S-VCSEL subject to DCOI is preferred to obtain high quality chaos.

For DCOI, two M-VCSELs can also possess different emitting frequencies and export different injection strengths, which may exert certain influences on the bandwidth and TDS of chaos from S-VCSEL. Therefore, it is essential to further explore the case in which two sets of injection parameters related with M-VCSEL1 and M-VCSEL2 are not matched. Fig. 6 shows the time series (first row), optical spectra (second row), power spectra (third row), and ACF curves (fourth row) of polarization-resolved chaos generated in S-VCSEL with DCOI for several representative parameter settings. Three different sets of injection parameters are presented for $\Delta\nu_1 = \Delta\nu_2 = -25$ GHz, $\eta_1 = \eta_2 = 50$ ns^{-1} (a1-a8), $\Delta\nu_1 = \Delta\nu_2 = -25$ GHz, $\eta_1 = 75$ ns^{-1} and $\eta_1 = 25$ ns^{-1} (b1-b8), and $\Delta\nu_1 = -25$ GHz and $\Delta\nu_2 = 10$ GHz, $\eta_1 = \eta_2 = 50$ ns^{-1} (c1-c8), respectively. When $\Delta\nu_1 = \Delta\nu_2 = -25$ GHz and $\eta_1 = \eta_2 = 50$ ns^{-1} (Fig. 6(a1)-(a8)), the time series of X-PC and Y-PC of S-VCSEL exhibit chaotic dynamics, the optical spectra maintain broad and an unremarkable peak around -25 GHz, the EBWs of X-PC and Y-PC reach 23.71 GHz and 23.66 GHz, respectively, and almost totally suppressed TDS for two orthogonal PCs can be achieved. As a result, the wideband chaos with total TDS concealment can be obtained in this case. In contrast, when $\Delta\nu_1 = \Delta\nu_2 = -25$ GHz, $\eta_1 = 75$ ns^{-1} and $\eta_2 = 25$ ns^{-1} (Fig. 6 (b1)-(b8)), the optical spectra possess a conspicuous peak around -25 GHz, the EBWs of X-PC and Y-PC are decreased significantly to 16.86 GHz and 16.99 GHz, respectively, and the ACF curves display obvious TDS, which is due to the fact that the relatively large η_1 dominates in the process of injection, and contributes to the injection locking effect. when $\Delta\nu_1 = -25$ GHz and $\Delta\nu_2 = 10$ GHz, $\eta_1 = \eta_2 = 50$ ns^{-1} (Fig. 6(c1)-(c8)), the optical spectra and power spectra are both broadened due to more frequency beating between M-VCSELs and the S-VCSEL, and the EBWs of two polarization-resolved outputs can be effectively improved by DCOI. However, the ACF curves still exhibit a high level σ compared to the result shown in Fig. 6(a1)-(a8). This indicates that different values of $\Delta\nu_1$ and $\Delta\nu_2$ (η_1 and η_2) can also affect the bandwidth and TDS of polarized chaos from S-VCSEL with DCOI.

In the following, Figure 7 presents evolution maps of EBW (first row) and σ (second row) of the polarization-resolved outputs for S-VCSEL with DCOI in the parameter space of η_1 and η_2, respectively. Here, $\Delta\nu_1$ and $\Delta\nu_2$ are all fixed at -25 GHz. Some representative lines are marked for the case that EBW (σ) of the polarized chaos is 20 GHz (0.1). As shown from the diagram, the high quality chaos with high EBW (EBW $>$ 20 GHz) and low σ ($\sigma < 0.1$) can be achieved within the special region of parameter space (25 ns^{-1} $< \eta_1 <$ 60 ns^{-1} and 25 ns^{-1} $< \eta_2 <$ 60 ns^{-1}). This indicates that under the given detuning condition, moderate injection values of η_1 or η_2 are desired to simultaneously achieve the bandwidth enhancement and TDS concealment of polarized chaos in S-VCSEL with DCOI. Nevertheless, when η_1 and η_2 are relatively small ($\eta_1 < 20$ ns^{-1} and $\eta_2 < 20$ ns^{-1}) or large ($\eta_1 > 75$ ns^{-1} and $\eta_2 > 75$ ns^{-1}), it is difficult to obtain the wideband polarized chaos with total TDS suppression.

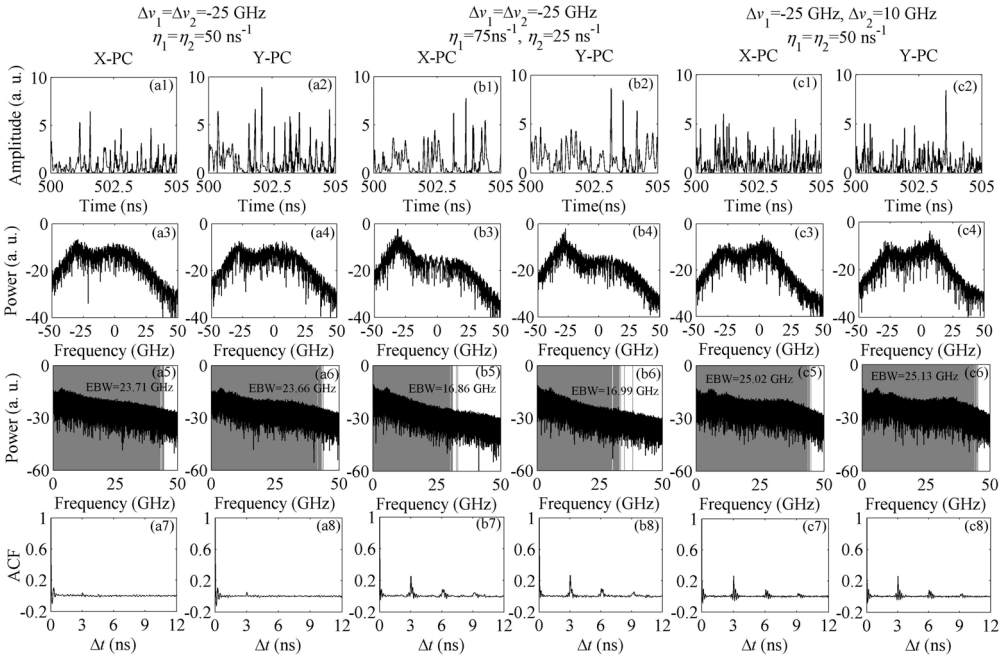

FIGURE 6. Time series (first row), optical spectra (second row), power spectra (third row), and corresponding ACF curves (fourth row) of polarization-resolved chaotic outputs from S-VCSEL with DCOI. (a1-a8): $\Delta\nu_1 = \Delta\nu_2 = -25$ GHz, $\eta_1 = \eta_2 = 50$ ns^{-1}; (b1-b8): $\Delta\nu_1 = \Delta\nu_2 = -25$ GHz, $\eta_1 = 75$ ns^{-1} and $\eta_1 = 25$ ns^{-1}; and (c1-c8): $\Delta\nu_1 = -25$ GHz and $\Delta\nu_2 = 10$ GHz, $\eta_1 = \eta_2 = 50$ ns^{-1}.

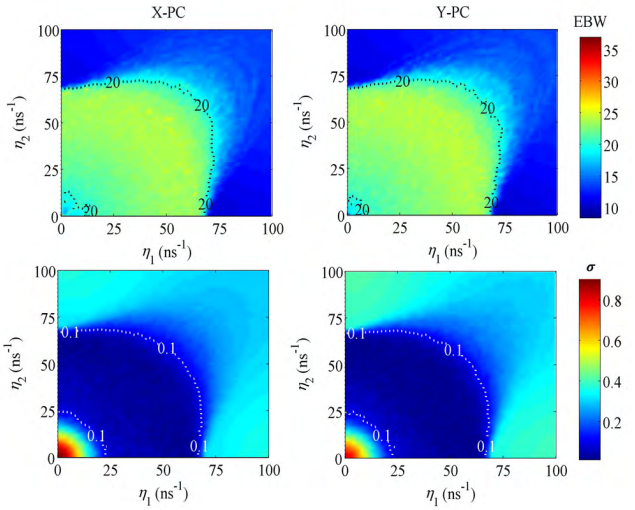

FIGURE 7. Evolution maps of EBW (first row) and σ (second row) of the polarization-resolved outputs from S-VCSEL with DCOI in the parameter space of η_1 and η_2, with $\Delta\nu_1 = \Delta\nu_2 = -25$ GHz.

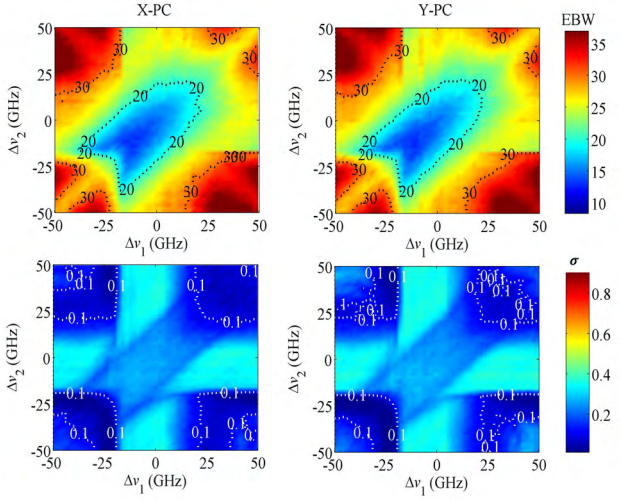

FIGURE 8. Evolution maps of EBW (first row) and σ (second row) of the polarization-resolved outputs from S-VCSEL with DCOI in the parameter space of $\Delta\nu_1$ and $\Delta\nu_2$, with $\eta_1 = \eta_2 = 50$ ns^{-1}.

In addition, it should be pointed out that, for the other cases with larger detuning, the wider overlapped parameter space will be satisfied to achieve the optimized EBW and TDS of polarized chaos from S-VCSEL.

Accordingly, the evolution maps of EBW (first row) and σ (second row) of the polarized chaos from S-VCSEL with DCOI in the parameter space of $\Delta\nu_1$ and $\Delta\nu_2$ are also displayed in Fig. 8. Here, η_1 and η_2 are fixed at 50 ns^{-1}. The black dashed lines in the first row diagrams of EBW represent the bandwidth location at 20 GHz and 30 GHz, respectively. The white dashed lines in the second row diagrams of TDS are marked for the case that σ is 0.1. As shown in the diagrams of EBW, the enhanced chaotic bandwidths more than 20 GHz for X-PC and Y-PC can be found over the wide parameter space, especially for the large detuning conditions of $\Delta\nu_1$ and $\Delta\nu_2$ where EBWs are

normally near or exceed 30 GHz. Correspondingly, as clearly shown in the diagrams of σ, satisfactory TDS suppression ($\sigma < 0.1$) for two polarized chaos can be achieved when Δv_1 and Δv_2 possess the relatively large values. Combining with the maps of EBW and σ presented here, the overlapped parameter regions for the bandwidth enhancement and TDS suppression of polarization-resolved chaos from S-VCSEL can be identified around the four corners of the parameter space of η_1 and η_2 in Fig. 8. In addition, when one of Δv_1 and Δv_2 is small, the wideband chaos with the low TDS cannot be realized. Therefore, it is necessary to choose appropriate values of Δv_1 and Δv_2 based on the combined guidance of wide bandwidth and low TDS characteristics.

IV. CONCLUSION

In summary, we have proposed to simultaneously enhance the bandwidth and suppress TDS of polarization-resolved chaos in a delayed-chaos VCSELs system, where a slave VCSEL is driven by DCOI from other two master VCSELs with optical feedback. Based on the spin-flip model (SFM), the bandwidth and TDS characteristics of polarization-resolved chaos generated in the slave VCSEL subject to DCOI are simulated theoretically after calculating the EBW and ACF. We find that, for the equivalent injection conditions, the DCIO is a more effective way to favor both bandwidth enhancement and TDS suppression under appropriate injection strength and frequency detuning than the case of SCOI, and high quality polarization-resolved chaos from the VCSEL subject to DCOI can be achieve in the wide injection parameter space. Further investigations show that different injection strength or frequency detuning of two paths of DCOI have significant effects on both the bandwidth and TDS of polarization-resolved chaos which can be effectively controlled through adjusting these injection parameters.

REFERENCES

[1] I. Fister, Jr., M. Perc, S. M. Kamal, and I. Fister, "A review of chaos-based firefly algorithms: Perspectives and research challenges," *Appl. Math. Comput.*, vol. 252, pp. 155–165, Feb. 2015.
[2] F. Nazarimehr, S. Jafari, S. M. R. H. Golpayegani, M. Perc, and J. C. Sprott, "Predicting tipping points of dynamical systems during a period-doubling route to chaos," *Chaos*, vol. 28, no. 7, Jul. 2018, Art. no. 073102.
[3] H. Someya, I. Oowada, H. Okumura, T. Kida, and A. Uchida, "Synchronization of bandwidth-enhanced chaos in semiconductor lasers with optical feedback and injection," *Opt. Express*, vol. 17, no. 22, pp. 19536–19543, Oct. 2009.
[4] J. A. Cramer and K. S. Booksh, "Chaos theory in chemistry and chemometrics: A review," *J. Chemometrics*, vol. 20, pp. 447–454, Nov./Dec. 2006.
[5] Z. Wang, Y. Moreno, S. Boccaletti, and M. Perc, "Vaccination and epidemics in networked populations—An introduction," *Chaos, Solitons Fractals*, vol. 103, pp. 177–183, Oct. 2017.
[6] J. N. Weiss, A. Garfinkel, M. L. Spano, and W. L. Ditto, "Chaos and chaos control in biology," *J. Clin. Invest.*, vol. 93, no. 4, pp. 1355–1360, Apr. 1994.
[7] B. R. R. Boaretto, R. C. Budzinski, T. L. Prado, J. Kurths, and S. R. Lopes, "Neuron dynamics variability and anomalous phase synchronization of neural networks," *Chaos, Interdiscipl. J. Nonlinear Sci.*, vol. 28, no. 10, Oct. 2018, Art. no. 106304.
[8] S. Boccaletti, C. Grebogi, Y.-C. Lai, H. Mancini, and D. Maza, "The control of chaos: Theory and applications," *Phys. Rep.*, vol. 329, no. 3, pp. 103–197, May 2000.
[9] A. Argyris *et al.*, "Chaos-based communications at high bit rates using commercial fibre-optic links," *Nature*, vol. 438, pp. 343–346, Nov. 2005.
[10] F. Ruiz-Oliveras, M. C. Soriano, P. Colet, and C. R. Mirasso, "Information encoding and decoding using unidirectionally coupled chaotic semiconductor lasers subject to filtered optical feedback," *IEEE J. Quantum Electron.*, vol. 45, no. 8, pp. 972–978, Aug. 2009.
[11] Y. Hong, M. W. Lee, J. Paul, P. S. Spencer, and K. A. Shore, "GHz bandwidth message transmission using chaotic vertical-cavity surface-emitting lasers," *J. Lightw. Technol.*, vol. 27, no. 22, pp. 5099–5105, Nov. 15, 2009.
[12] I. V. Ermakov, S. T. Kingni, V. Z. Tronciu, and J. Danckaert, "Chaotic semiconductor ring lasers subject to optical feedback: Applications to chaos-based communications," *Opt. Commun.*, vol. 286, pp. 265–272, Jan. 2013.
[13] I. Reidler, Y. Aviad, M. Rosenbluh, and I. Kanter, "Ultrahigh-speed random number generation based on a chaotic semiconductor laser," *Phys. Rev. Lett.*, vol. 103, no. 2, Jul. 2009, Art. no. 024102.
[14] A. Wang, P. Li, J. Zhang, J. Zhang, L. Li, and Y. Wang, "4.5 Gbps high-speed real-time physical random bit generator," *Opt. Express*, vol. 21, no. 17, pp. 20452–20462, Aug. 2013.
[15] N. Li *et al.*, "Two approaches for ultrafast random bit generation based on the chaotic dynamics of a semiconductor laser," *Opt. Express*, vol. 22, no. 6, pp. 6634–6646, Mar. 2014.
[16] F.-Y. Lin and J.-M. Liu, "Diverse waveform generation using semiconductor lasers for radar and microwave applications," *IEEE J. Quantum Electron.*, vol. 40, no. 6, pp. 682–689, Jun. 2004.
[17] F.-Y. Lin and J.-M. Liu, "Chaotic lidar," *IEEE J. Sel. Topics Quantum Electron.*, vol. 10, no. 5, pp. 991–997, Sep./Oct. 2004.
[18] Y. Wang, B. Wang, and A. Wang, "Chaotic correlation optical time domain reflectometer utilizing laser diode," *IEEE Photon. Technol. Lett.*, vol. 20, no. 19, pp. 1636–1638, Oct. 1, 2008.
[19] K. Hirano *et al.*, "Fast random bit generation with bandwidth-enhanced chaos in semiconductor lasers," *Opt. Express*, vol. 18, no. 6, pp. 5512–5524, Mar. 2010.
[20] D. Rontani, A. Locquet, M. Sciamanna, D. S. Citrin, and S. Ortin, "Time-delay identification in a chaotic semiconductor laser with optical feedback: A dynamical point of view," *IEEE J. Quantum Electron.*, vol. 45, no. 7, pp. 879–891, Jul. 2009.
[21] J.-G. Wu *et al.*, "Time delay signature concealment of optical feedback induced chaos in an external cavity semiconductor laser," *Opt. Express*, vol. 18, no. 7, pp. 6661–6666, Mar. 2010.
[22] F.-Y. Lin and J.-M. Liu, "Ambiguity functions of laser-based chaotic radar," *IEEE J. Quantum Electron.*, vol. 40, no. 12, pp. 1732–1738, Dec. 2004.
[23] A. Uchida *et al.*, "Fast physical random bit generation with chaotic semiconductor lasers," *Nature Photon.*, vol. 2, no. 12, pp. 728–732, 2008.
[24] M. W. Lee, P. Rees, K. A. Shore, S. Ortin, L. Pesquera, and A. Valle, "Dynamical characterisation of laser diode subject to double optical feedback for chaotic optical communications," *IEE Proc.-Optoelectron.*, vol. 152, no. 2, pp. 97–102, Apr. 2005.
[25] Y. S. Lin, "Enhancing the relaxation oscillation frequency of a chaotic semiconductor laser transmitter using optical dual-feedback light," *Opt. Commun.*, vol. 283, no. 17, pp. 3305–3309, Sep. 2010.
[26] J. G. Wu, G. Q. Xia, and Z. M. Wu, "Suppression of time delay signatures of chaotic output in a semiconductor laser with double optical feedback," *Opt. Express*, vol. 17, no. 22, pp. 20124–20133, 2009.
[27] N. Oliver, M. C. Soriano, D. W. Sukow, and I. Fischer, "Dynamics of a semiconductor laser with polarization-rotated feedback and its utilization for random bit generation," *Opt. Lett.*, vol. 36, no. 23, pp. 4632–4634, 2011.
[28] S.-S. Li, Q. Liu, and S.-C. Chan, "Distributed feedbacks for time-delay signature suppression of chaos generated from a semiconductor laser," *IEEE Photon. J.*, vol. 4, no. 5, pp. 1930–1935, Oct. 2012.
[29] A.-B. Wang, Y.-C. Wang, and J.-F. Wang, "Route to broadband chaos in a chaotic laser diode subject to optical injection," *Opt. Lett.*, vol. 34, no. 8, pp. 1144–1146, Mar. 2009.
[30] N. Li *et al.*, "Photonic generation of wideband time-delay-signature-eliminated chaotic signals utilizing an optically injected semiconductor laser," *IEEE J. Quantum Electron.*, vol. 48, no. 10, pp. 1339–1345, Oct. 2012.
[31] N. Li, W. Pan, S. Xiang, L. Yan, B. Luo, and X. Zou, "Loss of time delay signature in broadband cascade-coupled semiconductor lasers," *IEEE Photon. Technol. Lett.*, vol. 24, no. 23, pp. 2187–2190, Dec. 1, 2012.

[32] J. Martin-Regalado, F. Prati, M. S. Miguel, and N. B. Abraham, "Polarization properties of vertical-cavity surface-emitting lasers," *IEEE J. Quantum Electron.*, vol. 33, no. 5, pp. 765–783, May 1997.
[33] F. Koyama, "Recent advances of VCSEL photonics," *J. Lightw. Technol.*, vol. 24, no. 12, pp. 4502–4513, Dec. 2006.
[34] Y. Hong, P. S. Spencer, and K. A. Shore, "Enhancement of chaotic signal bandwidth in vertical-cavity surface-emitting lasers with optical injection," *J. Opt. Soc. Amer. B, Opt. Phys.*, vol. 29, no. 3, pp. 415–419, Mar. 2012.
[35] P. Pérez and A. Valle, "Enhancement of chaotic signal bandwidth in VCSELs induced by polarized optical injection," *IEEE J. Quantum Electron.*, vol. 51, no. 6, Jun. 2015, Art. no. 2400207.
[36] A. Quirce, A. Valle, H. Thienpont, and K. Panajotov, "Enhancement of chaos bandwidth in VCSELs induced by simultaneous orthogonal optical injection and optical feedback," *IEEE J. Quantum Electron.*, vol. 52, no. 10, Oct. 2016, Art. no. 2400609.
[37] Y. Hong, P. S. Spencer, and K. A. Shore, "Wideband chaos with time-delay concealment in vertical-cavity surface-emitting lasers with optical feedback and injection," *IEEE J. Quantum Electron.*, vol. 50, no. 4, pp. 236–242, Apr. 2014.
[38] Y. Hong, A. Quirce, B. Wang, S. Ji, K. Panajotov, and P. S. Spencer, "Concealment of chaos time-delay signature in three-cascaded vertical-cavity surface-emitting lasers," *IEEE J. Quantum Electron.*, vol. 52, no. 8, Aug. 2016, Art. no. 2400508.
[39] S. Y. Xiang *et al.*, "Wideband unpredictability-enhanced chaotic semiconductor lasers with dual-chaotic optical injections," *IEEE J. Quantum Electron.*, vol. 48, no. 8, pp. 1069–1076, Aug. 2012.
[40] N. Li, W. Pan, A. Locquet, and D. S. Citrin, "Time-delay concealment and complexity enhancement of an external-cavity laser through optical injection," *Opt. Lett.*, vol. 40, no. 19, pp. 4416–4419, Oct. 2015.
[41] S. Ji and Y. Hong, "Effect of bias current on complexity and time delay signature of chaos in semiconductor laser with time-delayed optical feedback," *IEEE J. Sel. Topics Quantum Electron.*, vol. 23, no. 6, Nov./Dec. 2017, Art. no. 1800706.
[42] F. Y. Lin and J. M. Liu, "Nonlinear dynamical characteristics of an optically injected semiconductor laser subject to optoelectronic feedback," *Opt. Commun.*, vol. 221, no. 1, pp. 173–180, Aug. 2003.
[43] F. Y. Lin, Y. K. Chao, and T. C. Wu, "Effective bandwidths of broadband chaotic signals," *IEEE J. Quantum Electron.*, vol. 48, no. 8, pp. 1010–1014, Aug. 2012.
[44] I. Gatare, M. Sciamanna, A. Locquet, and K. Panajotov, "Influence of polarization mode competition on the synchronization of two unidirectionally coupled vertical-cavity surface-emitting lasers," *Opt. Lett.*, vol. 32, no. 12, pp. 1629–1631, Jun. 2007.
[45] J. J. Chen *et al.*, "Generation of polarization-resolved wideband unpredictability-enhanced chaotic signals based on vertical-cavity surface-emitting lasers subject to chaotic optical injection," *Opt. Express*, vol. 23, no. 6, pp. 7173–7183, Mar. 2015.

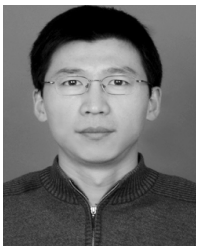

JIAN-JUN CHEN was born in Shihezi, Xinjiang, China, in 1977. He received the B.Sc. degree in physics from Xinjiang Normal University, Ürümqi, Xinjiang, in 2001, and the M.Sc. and Ph.D. degrees in optics from Southwest University, Chongqing, China, in 2008 and 2017, respectively.

He is currently an Associate Professor with the School of Medical Engineering and Technology, Xinjiang Medical University. His current research interests include chaotic time series analysis and nonlinear dynamics of semiconductor lasers.

YING-NI DUAN was born in Huaxian, Shanxi, China, in 1984. She received the B.Sc. degree in physics, the M.Sc. degree in condensed matter physics, and the Ph.D. degree in semiconductor physics from Shanxi Normal University, Xi'an, Shanxi, China, in 2006, 2009, and 2016, respectively.

She is currently an Associate Professor with the School of Medical Engineering and Technology, Xinjiang Medical University, Ürümqi. Her current research interests focus on nonlinear interaction among atomic, molecular, and photon and thermal properties of low-dimensional systems.

LIN-FU LI was born in Sheqi, Hennan, China, in 1981. He received the B.Sc. and Ph.D. degrees in physics from Southwest University, Chongqing, China, in 2005 and 2008, respectively, and the Ph.D. degree in optical engineering from Fudan University, Shanghai, China, in 2015.

He is currently an Associate Professor with the School of Mechatronics Engineering, Guizhou Minzu University, Guiyang. His current research interests include the nonlinear dynamics of semiconductor lasers.

ZHU-QIANG ZHONG was born in Chongqing, China, in 1988. He received the B.Sc. degree in information and communication engineering and the M.Sc. and Ph.D. degrees in optic communication from Southwest University, Chongqing, China, in 2011, 2014, and 2017, respectively.

He is currently a Lecturer with the School of Science, Chongqing University of Technology, Chongqing. His current research interests include the nonlinear dynamics of semiconductor lasers, optical chaos generation, and optical chaos communication.